Inorg. Chem. **2008**, *47*, 8101−8111

Facile Synthesis and Functionality-Dependent Electrochemistry of Fe-Only Hydrogenase Mimics

Gang Si, Wen-Guang Wang, Hong-Yan Wang, Chen-Ho Tung, and Li-Zhu Wu*

Key Laboratory of Photochemical Conversion and Optoelectronic Materials, Technical Institute of Physics and Chemistry & Graduate University, The Chinese Academy of Sciences, Beijing 100190, People's Republic of China

Received April 16, 2008

A series of azadithiolate (adt)-bridged Fe-only hydrogenase model complexes, $Fe_2(CO)_6(\mu\text{-adt})C_6H_4I$-4 (**1**), $Fe_2(CO)_6(\mu\text{-adt})C_6H_4C{\equiv}CR$ [R = $C_6H_4NO_2$-4 (**2**), C_6H_4CHO-4 (**3**), $C_6H_4NH_2$-4 (**4**), C_6H_4COOH-4 (**5**), $C_6H_4COOCH_2CH_3$-4 (**6**), C_6H_4F-4 (**7**), C_6H_5 (**8**), $C_6H_4OCH_3$-4 (**9**), $C_6H_4N(CH_3)_2$-4 (**10**)], $[Fe_2(CO)_5(PPh_3)(\mu\text{-adt})C_6H_4I$-4 (**11**), and $Fe_2(CO)_5(PPh_3)(\mu\text{-adt})C_6H_4C{\equiv}CC_6H_4NO_2$-4 (**12**), have been synthesized in high yields under mild conditions. The linear geometry and rigidity of a triple bond act as an effective bridge to anchor a functionality ranging from electron-donating to electron-accepting, even coordinative groups in the adt model complexes. X-ray crystal analysis of **2**, **3**, and **6**−**12** reveals that the model complexes retain the butterfly structure of Fe_2S_2 model analogues. A rigid phenylacetylene offers excellent control over the distance between the functional group and the active site of Fe_2S_2 model complexes. The unusual Fe−Fe distance and the angles found in the molecular packing of **6** are originated from the intriguing intermolecular C−H···O and C−H···S interactions. More importantly, electrochemical studies reveal that all of the complexes can catalyze electrochemical reduction of protons to molecular hydrogen, but the reduction potential for the electron-transfer step can be remarkably altered by the functionality R. The electroreductively active nitro group in **2** and **12** displays the enhanced current at a potential substantially less negative than the reduction of $[Fe^IFe^I] + e^- \rightarrow [Fe^IFe^0]$, which is most accessible and becomes the initial step. For complex **3**, the second reduction peak for the electron-transfer step involves the contribution from the aldehyde functionality. As the electroreductively inactive groups are incorporated, the reduction process of $[Fe^IFe^I] + e^- \rightarrow [Fe^IFe^0]$ appears first and the second reduction peak for the electron-transfer step from the $[Fe^IFe^0] + e^- \rightarrow [Fe^0Fe^0]$ process for **4**−**10** is clearly observed. Therefore, the order of electron and proton uptake is closely related to the electroreductively active functionality, R. Varying the nature of the functionality R leads to the electron-transfer step changes from the reduction of the electroreductively active R group to the active site of Fe_2S_2 model complexes subsequently. Accordingly, notwithstanding, acetic acid is too weak to protonate the series of **2**−**12**, different reduction pathways can be followed, and the electrochemically catalyzed behavior may occur at different reduction levels.

Introduction

Fe-only hydrogenase, a H_2 evolution system in nature, can catalyze the reversible reduction of protons to molecular hydrogen at neutral pH and at relatively low potential (ca. −0.4 V vs NHE) with high efficiency (6000−9000 molecules of H_2 s^{-1} per site).[1] The elucidation of the crystal structure of hydrogenases, isolated from *Clostridium pasteurianum*[2a] and *Desulfovibrio desulfuricans*,[2b] stimulates chemists to model the active site. A large number of synthetic model complexes featuring two dithiolate-bridged $[Fe^IFe^I]$ centers and six carbonyl ligands that closely resemble the enzyme's active site (Scheme 1) have been pursued to mimic the structure and functionality of the hydrogenase, to understand the mechanism of stepwise

Scheme 1. (a) Basic Structure of the Fe-Only Hydrogenase (X = CH_2, NH, O) and (b) Synthetic Model Complexes of the Fe-Only Hydrogenase (Y = CH_2, CHR, NH, NR, O, S)

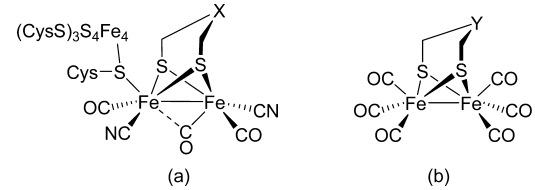

* To whom correspondence should be addressed. E-mail: lzwu@mail.ipc.ac.cn.

10.1021/ic800676y CCC: $40.75
Published on Web 08/19/2008

proton reduction in the active site of Fe_2S_2 analogues, and to construct biomimetic catalyst systems.[3]

From a synthetic point of view, two different strategies, substitution of carbonyl groups and modification of dithiolate linkers, have been employed for the preparation of Fe_2S_2 model complexes. For the first approach, electron-donating ligands, such as CN^-,[4] phosphorus,[5] CNR,[6] N-heterocyclic carbene,[7] and 1,10-phenanthroline,[8] are introduced by CO displacement. Mono- and disubstituted Fe_2S_2 model complexes that exhibit electrochemically catalytic characteristics have been reported. The second strategy involves the variation of the dithiolate linker, including propyldithiolate (pdt),[9] azadithiolate (adt),[10−12] oxadithiolate,[13] and thiadithiolate[14] bridges. Among them, the modification of the adt-bridged Fe_2S_2 clusters has been scrutinized because the importance of the nitrogen heteroatom in the bridge to its potential for protonation in its position close to the active site, which offered a thermodynamically and kinetically favorable pathway for hydrogen evolution, was proposed.[11,15] Nonetheless, the synthesis is not straightforward as expected because the Fe_2S_2 cluster is always sensitive and apt to decomposition. As examples of important synthetic intermediates, an aniline-substituted model complex could be produced only in a 20% yield via a direct reaction of [(μ-SH)$Fe_2(CO)_6$] with a premixed tetrahydrofuran (THF) solution of paraformaldehyde and *p*-phenylenediamine. Alternatively, it was successfully prepared by Sun and co-workers in a reasonable yield using a reduction of the 4-nitrobenzene-substituted model complex with Pd/C/H_2 under 0.4 MPa.[12c] A benzaldehyde-substituted adt complex, a precursor for covalently bonding a porphyrin photosensitizer, was recently obtained in a yield of 32%.[12d] Carboxylic acid-functionalized

(1) (a) Adams, M. W. W. *Biochim. Biophys. Acta* **1990**, *1020*, 115–145. (b) Holm, R. H.; Kennepohl, P.; Solomon, E. I. *Chem. Rev.* **1996**, *96*, 2239–2314. (c) Peters, J. W. *Curr. Opin. Struct. Biol.* **1999**, *9*, 670–676. (d) Frey, M. *ChemBioChem* **2002**, *3*, 153–160. (e) Tye, J. W.; Hall, M. B.; Darensbourg, M. Y. *Proc. Natl. Acad. Sci. U.S.A.* **2005**, *102*, 16911–16912.

(2) (a) Peters, J. W.; Lanzilotta, W. N.; Lemon, B. J.; Seefeldt, L. C. *Science* **1998**, *282*, 1853–1858. (b) Nicolet, Y.; Piras, C.; Legrand, P.; Hatchikian, C. E.; Fontecilla-Camps, J. C. *Structure* **1999**, *7*, 13–23.

(3) (a) Darensbourg, M. Y.; Lyon, E. J.; Smee, J. J. *Coord. Chem. Rev.* **2000**, *206−207*, 533–561. (b) Chong, D.; Georgakaki, I. P.; Mejia-Rodriguez, R.; Sanabria-Chinchilla, J.; Soriaga, M. P.; Darensbourg, M. Y. *Dalton Trans.* **2003**, *21*, 4158–4163. (c) Evans, D. J.; Pickett, C. J. *Chem. Soc. Rev.* **2003**, *32*, 268–275. (d) Georgakaki, I. P.; Thomson, L. M.; Lyon, E. J.; Hall, M. B.; Darensbourg, M. Y. *Coord. Chem. Rev.* **2003**, *238−239*, 255–266. (e) Rauchfuss, T. B. *Inorg. Chem.* **2004**, *43*, 14–26. (f) Song, L.-C. *Acc. Chem. Res.* **2005**, *38*, 21–28. (g) Artero, V.; Fontecave, M. *Coord. Chem. Rev.* **2005**, *249*, 1518–1535. (h) Best, S. P. *Coord. Chem. Rev.* **2005**, *249*, 1536–1554. (i) Liu, X.; Ibrahim, S. K.; Tard, C.; Pickett, C. J. *Coord. Chem. Rev.* **2005**, *249*, 1641–1652. (j) Sun, L.; Åkermark, B.; Ott, S. *Coord. Chem. Rev.* **2005**, *249*, 1653–1663. (k) Capon, J.-F.; Gloaguen, F.; Schollhammer, P.; Talarmin, J. *Coord. Chem. Rev.* **2005**, *249*, 1664–1676.

(4) (a) Le Cloirec, A.; Best, S. P.; Borg, S.; Davies, S. C.; Evans, D. J.; Hughes, D. L.; Pickett, C. J. *Chem. Commun.* **1999**, *22*, 2285–2286. (b) Schmidt, M.; Contakes, S. M.; Rauchfuss, T. B. *J. Am. Chem. Soc.* **1999**, *121*, 9736–9737. (c) Lyon, E. J.; Georgakaki, I. P.; Reibenspies, J. H.; Darensbourg, M. Y. *Angew. Chem., Int. Ed.* **1999**, *38*, 3178–3180. (d) Gloaguen, F.; Lawrence, J. D.; Schmidt, M.; Wilson, S. R.; Rauchfuss, T. B. *J. Am. Chem. Soc.* **2001**, *123*, 12518–12527.

(5) (a) Zhao, X.; Georgakaki, I. P.; Miller, M. L.; Yarbrough, J. C.; Darensbourg, M. Y. *J. Am. Chem. Soc.* **2001**, *123*, 9710–9711. (b) Zhao, X.; Georgakaki, I. P.; Miller, M. L.; Mejia-Rodriguez, R.; Chiang, C.-Y.; Darensbourg, M. Y. *Inorg. Chem.* **2002**, *41*, 3917–3928. (c) Mejia-Rodriguez, R.; Chong, D.; Reibenspies, J. H.; Soriaga, M. P.; Darensbourg, M. Y. *J. Am. Chem. Soc.* **2004**, *126*, 12004–12014. (d) Dong, W.; Wang, M.; Liu, X.; Jin, K.; Li, G.; Wang, F.; Sun, L. *Chem. Commun.* **2006**, *3*, 305–306. (e) Hou, J.; Peng, X.; Zhou, Z.; Sun, S.; Zhao, X.; Gao, S. *J. Organomet. Chem.* **2006**, *691*, 4633–4640. (f) Gao, W.; Liu, J.; Åkermark, B.; Sun, L. *Inorg. Chem.* **2006**, *45*, 9169–9171. (g) Justice, A. K.; Rauchfuss, T. B.; Wilson, S. R. *Angew. Chem., Int. Ed.* **2007**, *46*, 6152–6154. (h) Justice, A. K.; Zampella, G.; De Gioia, L.; Rauchfuss, T. B. *Chem. Commun.* **2007**, *20*, 2019–2021. (i) Ezzaher, S.; Capon, J-F.; Gloaguen, F.; Pétillon, F. Y.; Schollhammer, P.; Talarmin, J. *Inorg. Chem.* **2007**, *46*, 3426–3428. (j) Morvan, D.; Capon, J.-F.; Gloaguen, F.; Schollhammer, P.; Talarmin, J. *Eur. J. Inorg. Chem.* **2007**, *28*, 5062–5068. (k) Gao, W.; Ekström, J.; Liu, J.; Chen, C.; Eriksson, L.; Weng, L.; Åkermark, B.; Sun, L. *Inorg. Chem.* **2007**, *46*, 1981–1991. (l) Adam, F. I.; Hogarth, G.; Richards, I.; Sanchez, B. E. *Dalton Trans.* **2007**, *24*, 2495–2498.

(6) (a) Lawrence, J. D.; Rauchfuss, T. B.; Wilson, S. R. *Inorg. Chem.* **2002**, *41*, 6193–6195. (b) Nehring, J. L.; Heinekey, D. M. *Inorg. Chem.* **2003**, *42*, 4288–4292. (c) Boyke, C. A.; Rauchfuss, T. B.; Wilson, S. R.; Rohmer, M.-M.; Bénard, M. *J. Am. Chem. Soc.* **2004**, *126*, 15151–15160. (d) Hou, J.; Peng, X.; Liu, J.; Gao, Y.; Zhao, X.; Gao, S.; Han, K. *Eur. J. Inorg. Chem.* **2006**, *22*, 4679–4686.

(7) (a) Capon, J.-F.; Hassnaoui, S. E.; Gloaguen, F.; Schollhammer, P.; Tarlarmin, J. *Organometallics* **2005**, *24*, 2020–2022. (b) Tye, J. W.; Lee, J.; Wang, H.-W.; Mejia-Rodriguez, R.; Reibenspies, J. H.; Hall, M. B.; Darensbourg, M. Y. *Inorg. Chem.* **2005**, *44*, 5550–5552. (c) Morvan, D.; Capon, J.-F.; Gloaguen, F.; Le Goff, A.; Marchivie, M.; Michaud, F.; Schollhammer, P.; Talarmin, J.; Yaouanc, J.-J.; Pichon, R.; Kervarec, N. *Organometallics* **2007**, *26*, 2042–2052. (d) Duan, L.; Wang, M.; Li, P.; Na, Y.; Wang, N.; Sun, L. *Dalton Trans.* **2007**, *13*, 1277–1283.

(8) Orain, P.-Y.; Capon, J.-F.; Kervaree, N.; Gloaguen, F.; Pétillon, F.; Pichon, R.; Schollhammer, P.; Tarlarmin, J. *Dalton Trans.* **2007**, *34*, 3754–3756.

(9) (a) Seyferth, D.; Henderson, R. S.; Song, L.-C. *J. Organomet. Chem.* **1980**, *192*, C1−C5. (b) Salyi, S.; Kriitikos, M.; Åkermark, B.; Sun, L. *Chem.−Eur. J.* **2003**, *9*, 557–560. (c) Wolpher, H.; Borgström, M.; Hammarström, L.; Bergquist, J.; Sundström, V.; Styring, S.; Sun, L.; Åkermark, B. *Inorg. Chem. Commun.* **2003**, *6*, 989–991.

(10) (a) Lawrence, J. D.; Li, H.; Rauchfuss, T. B. *Chem. Commun.* **2001**, *16*, 1482–1483. (b) Lawrence, J. D.; Li, H.; Rauchfuss, T. B.; Bénard, M.; Rohmer, M.-M. *Angew. Chem., Int. Ed.* **2001**, *40*, 1768–1771. (c) Song, L.-C.; Yin, B.-S.; Li, Y.-L.; Zhao, L.-Q.; Ge, J.-H.; Yang, Z.-Y.; Hu, Q.-M. *Organometallics* **2007**, *26*, 4921–4929. (d) Song, L.-C.; Tang, M.-Y.; Mei, S.-Z.; Huang, J.-H.; Hu, Q.-M. *Organometallics* **2007**, *26*, 1575–1577. (e) Song, L.-C.; Wang, L.-X.; Yin, B.-S.; Li, Y.-L.; Zhang, X.-G.; Zhang, Y.-W.; Luo, X.; Hu, Q.-M. *Eur. J. Inorg. Chem.* **2008**, *2*, 291–297. (f) Jiang, S.; Liu, J.; Sun, L. *Inorg. Chem. Commun.* **2006**, *9*, 290–292. (g) Cui, H.; Wang, M.; Dong, W.; Duan, L.; Li, P.; Sun, L. *Polyhedron* **2007**, *26*, 904–910. (h) Capon, J.-F.; Ezzaher, S.; Gloaguen, F.; Pétillon, F. Y.; Schollhammer, P.; Talarmin, J.; Davin, T. J.; McGrady, J. E.; Muir, K. W. *New J. Chem.* **2007**, *31*, 2052–2064. (i) Capon, J.-F.; Ezzaher, S.; Gloaguen, F.; Pétillon, F. Y.; Schollhammer, P.; Talarmin, J. *Chem.−Eur. J.* **2008**, *14*, 1954–1964.

(11) (a) Ott, S.; Kritikos, M.; Åkermark, B.; Sun, L.; Lomoth, R. *Angew. Chem., Int. Ed.* **2004**, *43*, 1006–1009. (b) Schwartz, L.; Eilers, G.; Eriksson, L.; Gogoll, A.; Lomoth, R.; Ott, S. *Chem. Commun.* **2006**, *5*, 520–522. (c) Eilers, G.; Schwartz, L.; Stein, M.; Zampella, G.; de Gioia, L.; Ott, S.; Lomoth, R. *Chem.−Eur. J.* **2007**, *13*, 7075–7084.

(12) (a) Ott, S.; Kritikos, M.; Åkermark, B.; Sun, L. *Angew. Chem., Int. Ed.* **2003**, *42*, 3285–3288. (b) Ott, S.; Borgström, M.; Kritikos, M.; Lomoth, R.; Bergquist, J.; Åkermark, B.; Hammarström, L.; Sun, L. *Inorg. Chem.* **2004**, *43*, 4683–4692. (c) Liu, T.; Wang, M.; Shi, Z.; Cui, H.; Dong, W.; Chen, J.; Åkermark, B.; Sun, L. *Chem.−Eur. J.* **2004**, *10*, 4474–4479. (d) Song, L.-C.; Tang, M.-Y.; Su, F.-H.; Hu, Q.-M. *Angew. Chem., Int. Ed.* **2006**, *45*, 1130–1133.

(13) (a) Li, H.; Rauchfuss, T. B. *J. Am. Chem. Soc.* **2002**, *124*, 726–727. (b) Song, L.-C.; Yang, Z.-Y.; Bian, H.-Z.; Hu, Q.-M. *Organometallics* **2004**, *23*, 3082–3084. (c) Song, L.-C.; Yang, Z.-Y.; Bian, H.-Z.; Liu, Y.; Wang, H.-T.; Liu, X.-F.; Hu, Q.-M. *Organometallics* **2005**, *24*, 6126–6135.

(14) (a) Song, L.-C.; Yang, Z.-Y.; Hua, Y.-J.; Wang, H.-T.; Liu, Y.; Hu, Q.-M. *Organometallics* **2007**, *26*, 2106–2110. (b) Windhager, J.; Görls, H.; Petzold, H.; Mloston, G.; Linti, G.; Weigand, W. *Eur. J. Inorg. Chem.* **2007**, *28*, 4462–4471.

(15) (a) Nicolet, Y.; Lemon, B. J.; Fontecilla-Camps, J. C.; Peters, J. W. *Trends Biochem. Sci.* **2000**, *25*, 138–143. (b) Nicolet, Y.; de Lacey, A. L.; Vernède, X.; Fernandez, V. M.; Hatchikian, E. C.; Fontecilla-Camps, J. C. *J. Am. Chem. Soc.* **2001**, *123*, 1596–1601. (c) Fan, J.-H.; Hall, M. B. *J. Am. Chem. Soc.* **2001**, *123*, 3828–3829.

Scheme 2. (a) Et_3BHLi, THF, −78 °C; (b) *N*,*N*-Bis(chloromethyl)-4-iodoaniline, −78 °C; (c) 4-Substituted Phenylacetylene (HC≡CR), THF/NEt_3, $Pd(PPh_3)_2Cl_2$, CuI, 50 °C; (d) PPh_3, Toluene, 80 °C; (e) 4-Nitrophenylacetylene, THF/NEt_3, $Pd(PPh_3)_2Cl_2$, CuI, 50 °C

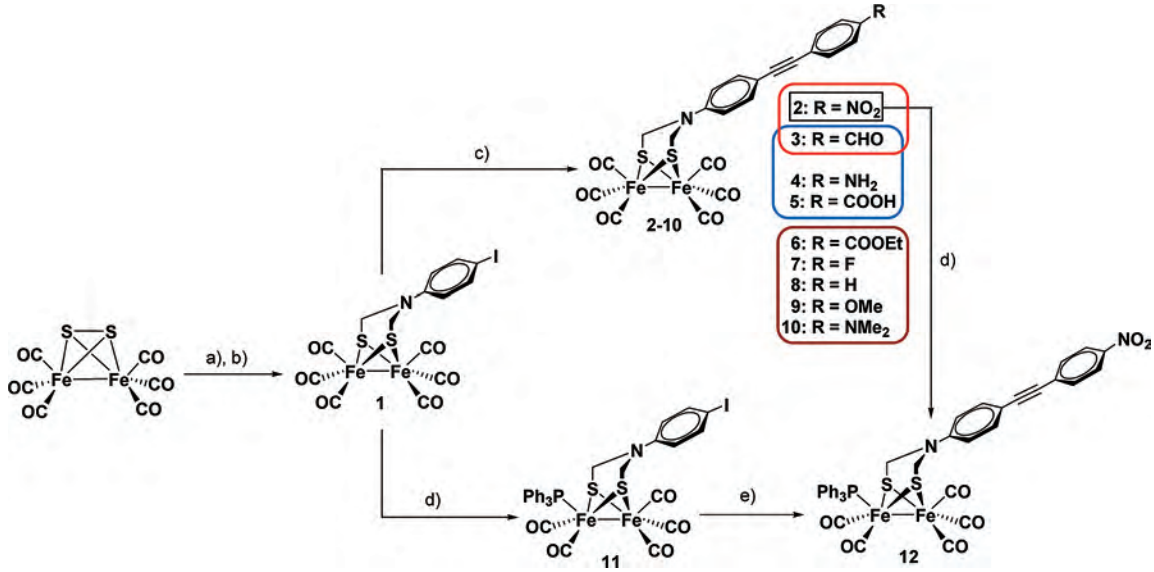

adt model complexes are yet to be achieved, while Rauchfuss and Darensbourg succeeded in the preparation of carboxylic acid-modified pdt-bridged Fe_2S_2 model complexes amenable to surface immobilization.[16] Thus, the development of synthetic protocols that are capable of affording a high yield of Fe_2S_2 model analogues and achieving catalytic activities comparable to that found in the natural system represents a major target from both synthetic and biomimetic points of view.

The Sonogashira reaction, the palladium-catalyzed cross-coupling reaction of terminal alkynes with aryl halides, has been a renaissance in the chemistry of aromatic alkynes.[17] Very recently, we found that the reaction is an efficient protocol to synthesize phenylacetylene-functionalized adt-bridged Fe_2S_2 complexes of hydrogenases.[18] An irreversible oxidation peak and a quasi-reversible reduction peak for $[Fe_2(CO)_6(\mu\text{-adt})C_6H_4C{\equiv}CC_6H_4NO_2\text{-}4]$ (**2**) were observed at 0.64 and −1.48 V vs Ag/Ag^+, respectively, which were tentatively assigned to $[Fe^IFe^I] \rightarrow [Fe^IFe^{II}] + e^-$ and $[Fe^IFe^I] + e^- \rightarrow [Fe^IFe^0]$ one-electron processes. Furthermore, the electrochemical proton reduction behavior of **2** was verified by cyclic voltammograms in the presence of acetic acid (HOAc). Much to our surprise, the first irreversible reduction peak for **2** was gradually anodic shifted to −1.25 V vs Ag/Ag^+ upon the addition of 28 equiv of HOAc. At the same time, the second quasi-reversible reduction peak gradually appeared at −1.52 V vs Ag/Ag^+ with enhanced current intensity. However, the nitrogen heteroatom in the adt bridge of phenylacetylene-functionalized complexes cannot be protonated by weak acid of HOAc, even at high concentration. This is consistent with the relative pK_a values of HOAc (pK_a = 22.3 in CH_3CN)[19] and of the protonated nitrogen bridgehead atom of closely related compounds ($7.6 < pK_a < 10.6$).[10b] The acid-dependent increase and anodic shift in the reduction current around −1.52 to −1.25 V vs Ag/Ag^+ suggest that reduction of **2** under these conditions first requires an electron-transfer step! Despite the fact that such a cyclic voltammetric behavior has been realized in several cases,[12c,18] little is known about the intimate mechanism of catalysis by the adt-bridged model complexes.

To gain insight into such an electrocatalytic proton reduction process, a series of model complexes, $Fe_2(CO)_6(\mu\text{-adt})C_6H_4C{\equiv}CR\text{-}4$ (**2**−**10**), $Fe_2(CO)_5(PPh_3)(\mu\text{-adt})C_6H_4I\text{-}4$ (**11**), and $Fe_2(CO)_5(PPh_3)(\mu\text{-adt})C_6H_4C{\equiv}CC_6H_4NO_2\text{-}4$ (**12**) (Scheme 2), have been designed and synthesized in this work. A rigid phenylacetylene is incorporated to satisfy the precise control over the spatial separation between the introduced R group and the active site of Fe_2S_2 model complexes. It is anticipated that (1) the Sonogashira reaction may simplify the synthetic procedures to afford the model complexes with substituted R groups ranging from electron-donating to electron-accepting. In particular, aniline-, benzaldehyde-, or carboxylic acid-functionalized adt-bridged model complexes could be prepared in higher yields under mild conditions as compared with those reported in the literature;[12c,d,16] (2) the linear and rigid triple bond may easily anchor functional groups in the adt-bridged complexes to avoid R substituent binding of the iron core of the complexes, and at the same time, the designed series may provide a base for systematically mechanistic investigation because the electrochemical reduction potential is known to depend significantly on the functional-group-involved molecular structure; (3) it has been known[5] that the electron-donating phosphine ligands render two iron active centers of Fe_2S_2 model complexes more

(16) (a) Volkers, P. I.; Rauchfuss, T. B.; Wilson, S. R. *Eur. J. Inorg. Chem.* **2006**, *23*, 4793–4799. (b) Vijaikanth, V.; Capon, J.-F.; Gloaguen, F.; Pétillon, F. Y.; Schollhammer, P.; Talarmin, J. *J. Organomet. Chem.* **2007**, *692*, 4177–4181. (c) Thomas, C. M.; Rüdiger, O.; Liu, T.; Carson, C. E.; Hall, M. B.; Darensbourg, M. Y. *Organometallics* **2007**, *26*, 3976–3984.

(17) (a) Sonogashira, K. In *Metal-Catalyzed Cross-Coupling Reactions*; Diederich, F., Stang, P. J. Eds.; Wiley-VCH: Weinheim, Germany, 1998. (b) Sonogashira, K. *J. Organomet. Chem.* **2002**, *653*, 46–49.

(18) Si, G.; Wu, L.-Z.; Wang, W.-G.; Ding, J.; Shan, X.-F.; Zhao, Y.-P.; Tung, C.-H.; Xu, M. *Tetrahedron Lett.* **2007**, *48*, 4775–4779.

(19) Izutzu, K. *Acid−Base Dissociation Constants in Dipolar Aprotic Solvents*; IUPAC Chemical Data Series No. 35; Blackwell Scientific Publications: Oxford, U.K., 1990.

nucleophilic. Here, **11** was chosen as an example to examine whether the coordinated phosphine ligand could influence the coupling reaction and electrocatalytic behavior for proton reduction.

In the present work, we report that the designed Fe_2S_2 model complexes **2**−**10**, including benzaldehyde, aniline, and carboxylic acid functional groups anchored at the Fe_2S_2 model complexes (**3**−**5**), can be prepared in high-to-excellent yields simply by the Sonogashira reaction. The direct reaction of **11** with 4-nitrophenylacetylene catalyzed by CuI and $Pd(PPh_3)_2Cl_2$ at room temperature results in **12** exclusively. X-ray crystal structural analysis of **2**, **3**, and **6**−**12** suggests that the model complexes retain the butterfly structure of Fe_2S_2 model analogues. A rigid phenylacetylene offers excellent control over the distance between the functional group and the active site of Fe_2S_2 model complexes. The intermolecular C−H···O and C−H···S hydrogen bonds are responsible for the molecular packing of **6** in the crystal lattices. More significantly, the linear geometry and rigidity of a triple bond act as an effective bridge to anchor a functionality ranging from electron-donating to electron-accepting, even coordinative groups in the adt model complexes. A comparison of the electrochemical properties of the reference compounds of $[(CH_3)_2NC_6H_4C{\equiv}CC_6H_4NO_2$-4] (**13**) and $[(CH_3)_2NC_6H_4C{\equiv}CC_6H_4CHO$-4] (**14**) reveals that the reduction potential for the electron-transfer step can be remarkably altered by the functionality R. Varying the nature of the functionality R on the phenyl ring leads to the electron-transfer step from the reduction of an electroreductively active group R to the active site of Fe_2S_2 analogues subsequently. As the electroreductively inactive groups are incorporated, the reduction process of $[Fe^IFe^I] + e^- \rightarrow [Fe^IFe^0]$ appears first and the second reduction peak for the electron-transfer step from the $[Fe^IFe^0] + e^- \rightarrow [Fe^0Fe^0]$ process is clearly observed. Notwithstanding, HOAc is too weak to protonate the series of **2**−**12**, different reduction pathways can be followed, and the electrochemically catalyzed behavior may occur at different reduction levels.

Experimental Section

Materials and Instrumentation. All reactions and operations were carried out in a dry argon atmosphere with standard Schelenk techniques. All solvents were dried and distilled prior to use according to the standard methods.[20] Paraformaldelyde, lithium triethylborohydride (Et_3BHLi), phenylacetylene, 4-fluorophenylacetylene, triphenylphosphine (PPh_3), 1-iodo-4-nitrobenzene, 4-bromobenzaldehyde, 4-methoxyphenylacetylene, 4-ethynylbenzenamine, and 4-nitrophenylacetylene were purchased from Aldrich and used as received. 4-Ethynylbenzoic acid, 4-ethynylbenzoate, 4-ethynylbenzaldehyde, and 4-ethynyl-*N*,*N*-dimethylbenzenamine were prepared according to the reported literature.[21] $Fe(CO)_5$ was purchased from Lanzhou Institute of Chemistry and Physics, The Chinese Academy of Sciences.

(20) Perrin, D. D.; Armarego, W. L. F. *Purification of Laboratory Chemicals*, 3rd ed.; Pergamon Press: New York, 1988.

(21) (a) Melissaris, A. P.; Litt, M. H. *J. Org. Chem.* **1992**, *57*, 6998–6999. (b) Belema, M.; Nguyen, V. N.; Zusi, F. C. *Tetrahedron Lett.* **2004**, *45*, 1693–1697. (c) Vicent, M. G. H.; Shetty, S. J.; Wickramasinghe, A.; Smith, K. M. *Tetrahedron Lett.* **2000**, *41*, 7623–7627. (d) Rodriiguez, J. G.; Ewquivias, J.; Lafuente, A.; Rubio, L. *Tetrahedron* **2006**, *62*, 3112–3122.

IR spectra were recorded on a Nicolet NEXUS 670 FT-IR spectrophotometer. ^1H and ^{13}C NMR spectra were run on a Bruker-400 spectrometer with tetramethylsilane (^1H), $CDCl_3$ (^{13}C), or DMSO-d_6 (^{13}C) as the internal standard, respectively. HR-ESI-MS was performed on a Bruker APEX III 7.0 T FTICR mass spectrometer combined with an Apollo ESI source. MALDI-TOF-MS was performed on a MicroFlex MALDI-TOF mass spectrometer (Bruker). Elemental analyses were determined on a FLASH EA1112 elemental analyzer. Electrochemical investigation was manipulated on a Princeton Applied Research potentionstat−galvanostat model 283. Acetonitrile (Fisher Chemicals, HPLC grade) used for the electrochemical performance was distilled under an argon atmosphere from CaH_2 and P_2O_5 in a stepwise manner followed by distillation from CaH_2 again immediately before use. A three-electrode system, a 3 mm glass carbon working electrode, a platinum wire counter electrode, and a nonaqueous Ag/Ag^+ reference electrode were used to measure the cyclic voltammograms. The working electrode was polished with a 0.05 μm alumina paste and sonicated for 15 min before use. The electrolyte solution, 0.1 M of n-Bu_4NPF_6 used as the electrolyte, was degassed with argon for 30 min before measurement. Gas chromatograms were recorded on a Shimadzu GC-14B.

Synthesis of $[Fe_2(CO)_6(\mu$-adt)$C_6H_4C{\equiv}CC_6H_4NO_2$-4] (2). To a well-degassed solution of iodophenyl-substituted model complex $Fe_2(CO)_6(\mu$-adt)C_6H_4I-4] (**1**)[12a,b] (0.10 mmol) and 4-nitrophenylacetylene (0.15 mmol) in 15 mL of THF/NEt_3 (5:1) were added successively $Pd(PPh_3)_2Cl_2$ (15 mg) and then CuI (5 mg). The mixture was concentrated in vacuo and filtered after stirring under an argon atmosphere at 40−50 °C for 3 h. The resulting black residue was further purified by column chromatography on silica gel (CH_2Cl_2/petroleum ether) to afford complex **2** as a red solid (yield 90%). HR-ESI-MS (*m*/*z*). Calcd for $[C_{22}H_{12}Fe_2N_2O_8S_2 + H^+]$: 608.8812 $(M + H)^+$. Found: 608.8787. ^1H NMR ($CDCl_3$, 400 MHz, δ ppm): 8.21 (d, J = 8.6 Hz, 2H), 7.64 (d, J = 8.5 Hz, 2H), 7.52 (d, J = 8.6 Hz, 2H), 6.74 (d, J = 8.5 Hz, 2H), 4.35 (s, 4H). ^{13}C NMR ($CDCl_3$, 100 MHz, δ ppm): 206.9, 146.9, 145.2, 133.9, 132.1, 130.8, 123.8, 115.5, 113.4, 95.3, 87.4, 49.6. Anal. Calcd for $C_{22}H_{12}Fe_2N_2O_8S_2$: C, 43.45; H, 1.99; N, 4.61. Found: C, 43.31; H, 2.06; N, 4.66. IR (KBr, ν cm^{-1}): ν(CO) 2073.5, 2033.8, 1993.4; ν(C≡C) 2210.8; $\nu(NO_2)$ 1513.9, 1341.0.

Synthesis of $[Fe_2(CO)_6(\mu$-adt)$C_6H_4C{\equiv}CC_6H_4CHO$-4] (3). Complex **3** was synthesized by a procedure similar to that for **2**, except that 4-formylphenylacetylene (0.15 mmol) was used in place of 4-nitrophenylacetylene. The mixture was concentrated in vacuo, and the black residue was subjected to column chromatography on silica gel (CH_2Cl_2/petroleum ether) to give complex **3** as a red solid (yield 83%). HR-ESI-MS (*m*/*z*). Calcd for $[C_{23}H_{13}Fe_2NO_7S_2 + H^+]$: 591.8918 $(M + H)^+$. Found: 591.8912. ^1H NMR ($CDCl_3$, 400 MHz, δ ppm): 10.01 (s, 1H), 7.86 (d, J = 7.7 Hz, 2H), 7.66 (d, J = 7.7 Hz, 2H), 7.52 (d, J = 8.2 Hz, 2H), 6.74 (d, J = 8.2 Hz, 2H), 4.34 (s, 4H). ^{13}C NMR ($CDCl_3$, 100 MHz, δ ppm): 206.9, 191.6, 144.9, 135.3, 133.8, 132.0, 130.1, 129.7, 115.5, 113.9, 93.9, 88.2, 49.6. Anal. Calcd for $C_{23}H_{13}Fe_2NO_7S_2$: C, 46.73; H, 2.22; N, 2.37. Found: C, 46.57; H, 2.07; N, 2.53. IR (KBr, ν cm^{-1}): ν(CO) 2074.6, 2033.2, 1995.5; ν(C≡C) 2208.2; ν(C═O) 1660.5.

Synthesis of $[Fe_2(CO)_6(\mu$-adt)$C_6H_4C{\equiv}CC_6H_4NH_2$-4] (4). Complex **4** was synthesized by a procedure similar to that for **2**, except that 4-ethynylbenzenamine (0.15 mmol) was used in place of 4-nitrophenylacetylene. The mixture was concentrated in vacuo, and the black residue was subjected to column chromatography on silica gel (CH_2Cl_2/petroleum ether) to give complex **4** as a red solid (yield 79%). HR-ESI-MS (*m*/*z*). Calcd for $[C_{22}H_{14}Fe_2N_2O_6S_2 + H^+]$: 578.9077 $(M + H)^+$. Found: 578.9059. ^1H NMR ($CDCl_3$, 400 MHz,

δ ppm): 7.45 (d, J = 8.6 Hz, 2H), 7.33 (d, J = 8.3 Hz, 2H), 6.69 (d, J = 8.6 Hz, 2H), 6.63 (d, J = 8.3 Hz, 2H), 4.33 (s, 4H), 3.80 (s, 2H). ^{13}C NMR ($CDCl_3$, 100 MHz, δ ppm): 207.0, 146.6, 143.9, 133.2, 133.0, 115.6, 115.5, 114.9, 113.1, 89.4, 87.3, 49.7. Anal. Calcd for $C_{22}H_{14}Fe_2N_2O_6S_2 \cdot {}^1/_3CH_2Cl_2$: C, 44.23; H, 2.44; N, 4.62. Found: C, 44.39; H, 2.40; N, 5.04. IR (KBr, ν cm^{-1}): ν(CO) 2074.3, 2032.9, 1993.8; ν(C≡C) 2210.0; ν(NH_2) 3411.6.

Synthesis of [$Fe_2(CO)_6$(μ-adt)C_6H_4C≡CC_6H_4COOH-4] (5). Complex **5** was synthesized by a procedure similar to that for **2**, except that 4-ethynylbenzoic acid (0.15 mmol) was used in place of 4-nitrophenylacetylene. The mixture was concentrated in vacuo, and the black residue was subjected to column chromatography on silica gel (CH_2Cl_2/CH_3OH) to give complex **5** as a red solid (yield 85%). HR-ESI-MS (*m*/*z*). Calcd for [$C_{23}H_{13}Fe_2NO_8S_2$ − H^+]: 605.8711 $(M - H)^+$. Found: 605.8691. ^{1}H NMR (DMSO-d_6, 400 MHz, δ ppm): 7.95 (d, J = 7.3 Hz, 2H), 7.63 (d, J = 7.3 Hz, 2H), 7.51 (d, J = 8.2 Hz, 2H), 6.70 (d, J = 8.2 Hz, 2H), 4.60 (s, 4H), 13.01 (br, 1H). ^{13}C NMR (DMSO-d_6, 100 MHz, δ ppm): 217.1, 166.9, 144.5, 133.3, 131.1, 129.5, 128.8, 127.1, 115.4, 111.9, 92.9, 87.6, 48.8. Anal. Calcd for $C_{23}H_{13}Fe_2NO_8S_2 \cdot {}^1/_3CH_2Cl_2$: C, 44.10; H, 2.17; N, 2.20. Found: C, 44.28; H, 2.58; N, 2.24. IR (CH_2Cl_2, ν cm^{-1}): ν(CO) 2074.7, 2034.9, 1994.4, 1969.0; ν(C≡C) 2205.9; ν(OH) 3393.6; ν(C═O) 1680.2.

Synthesis of [$Fe_2(CO)_6$(μ-adt)C_6H_4C≡CC_6H_4COOCH_2CH_3-4] (6). Complex **6** was synthesized by a procedure similar to that for **2**, except that ethyl 4-ethynylbenzoate (0.15 mmol) was used in place of 4-nitrophenylacetylene. The mixture was concentrated in vacuo, and the black residue was subjected to column chromatography on silica gel (CH_2Cl_2/petroleum ether) to give complex **6** as a red solid (yield 83%). HR-ESI-MS (*m*/*z*). Calcd for [$C_{25}H_{17}Fe_2NO_8S_2$ + H^+]: 635.9173 $(M + H)^+$. Found: 635.9181. ^{1}H NMR ($CDCl_3$, 400 MHz, δ ppm): 8.03 (d, J = 7.5 Hz, 2H), 7.58 (d, J = 7.5 Hz, 2H), 7.52 (d, J = 8.0 Hz, 2H), 6.75 (d, J = 8.0 Hz, 2H), 4.34 (s, 4H), 4.39 (q, J = 7.2 Hz, 2H), 1.41 (t, J = 7.2 Hz, 3H). ^{13}C NMR ($CDCl_3$, 100 MHz, δ ppm): 207.0, 166.3, 144.7, 133.7, 132.5, 131.4, 129.6, 128.7, 115.5, 114.2, 92.6, 88.3, 61.3, 49.6, 14.5. Anal. Calcd for $C_{25}H_{17}Fe_2NO_8S_2$: C, 47.27; H, 2.70; N, 2.21. Found: C, 47.69; H, 3.02; N, 2.64. IR (KBr, νcm^{-1}): ν(CO) 2074.9, 2034.2, 1997.1; ν(C≡C) 2214.9, ν(C═O) 1717.8.

Synthesis of [$Fe_2(CO)_6$(μ-adt)C_6H_4C≡CC_6H_4F-4] (7). Complex **7** was synthesized by a procedure similar to that for **2**, except that ethynyl-4-fluorobenzene (0.15 mmol) was used in place of 4-nitrophenylacetylene. The mixture was concentrated in vacuo, and the black residue was subjected to column chromatography on silica gel (CH_2Cl_2/petroleum ether) to give complex **7** as a red solid (yield 86%). HR-ESI-MS (*m*/*z*). Calcd for [$C_{22}H_{12}FFe_2NO_6S_2$ + H^+]: 581.8874 $(M + H)^+$. Found: 581.8879. ^{1}H NMR ($CDCl_3$, 400 MHz, δ ppm): 7.49−7.46 (m, 4H), 7.04 (t, 2H), 6.72 (d, J = 6.9 Hz, 2H), 4.34 (s, 4H). ^{13}C NMR ($CDCl_3$, 100 MHz, δ ppm): 207.0, 163.7, 161.3, 144.4, 133.5, 119.8, 115.9, 115.7, 115.5, 114.6, 89.1, 87.7, 49.6. Anal. Calcd for $C_{22}H_{12}FFe_2NO_6S_2$: C, 45.47; H, 2.08; N, 2.41. Found: C, 45.17; H, 2.10; N, 2.32. IR (KBr, ν cm^{-1}): ν(CO) 2073.7, 2034.1, 1997.1; ν(C≡C) 2214.1.

Synthesis of [$Fe_2(CO)_6$(μ-adt)C_6H_4C≡CC_6H_5] (8). Complex **8** was synthesized by a procedure similar to that for **2**, except that phenylacetylene (0.15 mmol) was used in place of 4-nitrophenylacetylene. The mixture was concentrated in vacuo, and the black residue was subjected to column chromatography on silica gel (CH_2Cl_2/petroleum ether) to give complex **8** as a red solid (yield 78%). HR-ESI-MS (*m*/*z*). Calcd for [$C_{22}H_{13}Fe_2NO_6S_2$ + H^+]: 563.8961 $(M + H)^+$. Found: 563.8974. ^{1}H NMR ($CDCl_3$, 400 MHz, δ ppm): 7.51−7.48 (m, 4H), 7.33 (m, 3H), 6.72 (d, J = 8.1 Hz, 2H), 4.34 (s, 4H). ^{13}C NMR ($CDCl_3$, 100 MHz, δ ppm): 207.0, 144.4−133.5, 131.6, 128.5, 128.1, 123.7, 115.5, 114.9, 89.5, 88.8, 49.6. Anal. Calcd for $C_{22}H_{13}Fe_2NO_6S_2$: C, 46.92; H, 2.33; N, 2.49. Found: C, 47.04; H, 2.47; N, 2.78. IR (KBr, ν cm^{-1}): ν(CO) 2071.6, 2034.9, 2007.4, 1985.6; ν(C≡C) 2209.3.

Synthesis of [$Fe_2(CO)_6$(μ-adt)C_6H_4C≡CC_6H_4OCH_3-4] (9). Complex **9** was synthesized by a procedure similar to that for **2**, except that 4-ethynylanisole (0.15 mmol) was used in place of 4-nitrophenylacetylene. The mixture was concentrated in vacuo, and the black residue was subjected to column chromatography on silica gel (CH_2Cl_2/petroleum ether) to give complex **9** as a red solid (yield 85%). HR-ESI-MS (*m*/*z*). Calcd for [$C_{23}H_{15}Fe_2NO_7S_2$ + H^+]: 593.9097 $(M + H)^+$. Found: 593.9050. ^{1}H NMR ($CDCl_3$, 400 MHz, δ ppm): 7.48−7.45 (m, 4H), 6.88 (d, J = 8.6 Hz, 2H), 6.71 (d, J = 8.6 Hz, 2H), 4.34 (s, 4H), 3.83 (s, 3H). ^{13}C NMR ($CDCl_3$, 100 MHz, δ ppm): 207.0, 159.6, 144.1, 133.3, 133.0, 115.8, 115.5, 115.2, 114.1, 88.7, 88.1, 55.4, 49.7, 14.47. Anal. Calcd for $C_{23}H_{15}Fe_2NO_7S_2$: C, 46.57; H, 2.55; N, 2.36. Found: C, 46.69; H, 2.65; N, 2.53. IR (KBr, ν cm^{-1}): ν(CO) 2083.1, 2031.3, 1998.4, 1963.4; ν(C≡C) 2208.0.

Synthesis of [$Fe_2(CO)_6$(μ-adt)C_6H_4C≡CC_6H_4N$(CH_3)_2$-4] (10). Complex **10** was synthesized by a procedure similar to that for **2**, except that 4-ethynyl-*N*,*N*-dimethylbenzenamine (0.15 mmol) was used in place of 4-nitrophenylacetylene. The mixture was concentrated in vacuo, and the black residue was subjected to column chromatography on silica gel (CH_2Cl_2/petroleum ether) to give complex **10** as a red solid (yield 80%). HR-ESI-MS (*m*/*z*). Calcd for [$C_{24}H_{18}Fe_2N_2O_6S_2$ + H^+]: 606.9391 $(M + H)^+$. Found: 606.9364. ^{1}H NMR ($CDCl_3$, 400 MHz, δ ppm): 7.45 (d, J = 8.6 Hz, 2H), 7.40 (d, J = 8.6 Hz, 2H), 6.69 (d, J = 8.6 Hz, 2H), 6.66 (d, J = 8.6 Hz, 2H), 4.33 (s, 4H), 2.99 (s, 6H). Anal. Calcd for $C_{24}H_{18}Fe_2N_2O_6S_2 \cdot {}^1/_3$[4-$(CH_3)_2NC_6H_4$C≡CC≡$CC_6H_4N(CH_3)_2$-4′]: C, 51.89; H, 3.58; N, 5.38. Found: C, 51.74; H, 3.74; N, 5.05. IR (KBr, ν cm^{-1}): ν(CO) 2074.3, 2027.9, 1991.3; ν(C≡C) 2213.5.

Synthesis of [$Fe_2(CO)_5(PPh_3)$(μ-adt)C_6H_4I-4] (11). To a well-degassed toluene solution of [(4-iodophenyl)(μ-adt)$Fe_2(CO)_6$] (0.10 mmol) was added trimethylamine *N*-oxide (0.10 mmol) and triphenyphosphine (0.12 mmol) with stirring under an argon atmosphere at 80 °C for 3 h. The mixture was concentrated in vacuo, and the black residue was subjected to column chromatography on silica gel (CH_2Cl_2/petroleum ether) to give a red solid **11** (yield 87%). MALDI-TOF-MS (*m*/*z*): 823.331. ^{1}H NMR ($CDCl_3$, 400 MHz, δ ppm): 7.72 (m, 6H), 7.45 (m, 9H), 7.37 (d, J = 8.6 Hz, 2H), 6.32 (d, J = 8.5 Hz, 2H), 3.96 (d, 2H), 2.92 (d, 2H). ^{13}C NMR ($CDCl_3$, 100 MHz, δ ppm): 212.9, 208.8, 146.1, 138.3, 135.8, 135.4, 133.8, 133.6, 130.5, 128.9, 128.8, 117.7, 81.4, 47.0. ^{31}P NMR ($CDCl_3$, δ ppm): 65.79. Anal. Calcd for $C_{23}H_{13}Fe_2NO_8S_2$: C, 45.23; H, 2.82; N, 1.70. Found: C, 45.15; H, 2.82; N, 1.82. IR (KBr, ν cm^{-1}): ν(CO) 2044.9, 1984.4, 1932.1.

Synthesis of [$Fe_2(CO)_5(PPh_3)$(μ-adt)C_6H_4C≡C$C_6H_4NO_2$-4)] (12). Complex **12** can be successfully achieved in the following two ways: (1) The procedure is similar to that for **2**, except that 4-nitrophenylacetylene (0.15 mmol) was reacted with **11**. The mixture was concentrated in vacuo, and the black residue was subjected to column chromatography on silica gel (CH_2Cl_2/petroleum ether) to give complex **12** as a red solid (yield 82%). (2) The direct reaction of **10** (0.10 mmol) with trimethylamine *N*-oxide (0.10 mmol) and triphenyphosphine (0.12 mmol) under an argon atmosphere at 80 °C for 4 h resulted in the formation of a black residue, which was further purified by column chromatography on silica gel (CH_2Cl_2/petroleum ether) to afford complex **12** in 85% yield. ^{1}H NMR ($CDCl_3$, 400 MHz, δ ppm): 8.19 (d, J = 8.6 Hz, 2H), 7.74 (m, 6H), 7.60 (d, J = 8.6 Hz, 2H), 7.44 (m, 9H), 7.38 (d, J = 8.6 Hz, 2H), 6.57 (d, J = 8.5 Hz, 2H), 4.10 (d, 2H),

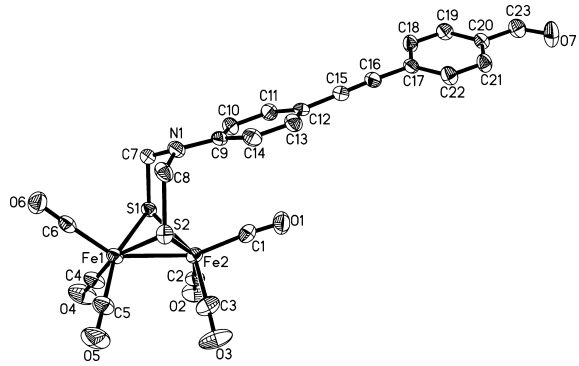

Figure 1. ORTEP view of **3** (ellipsoids at the 30% probability level).

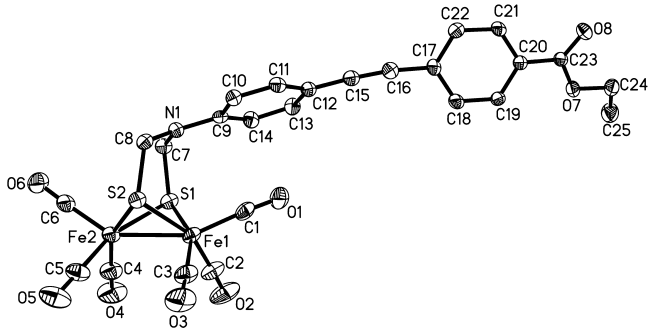

Figure 2. ORTEP view of **6** (ellipsoids at the 30% probability level).

2.96 (d, 2H). ^{13}C NMR (DMSO-d_6, 100 MHz, δ ppm): 212.8, 208.7, 146.4, 135.7, 135.3, 133.8, 133.6, 132.0, 131.0, 130.6, 130.4, 128.9, 128.8, 127.8, 123.9, 123.8, 114.9, 112.1, 95.9, 87.1, 49.6, 29.9. ^{31}P NMR ($CDCl_3$, δ ppm): 65.78. Anal. Calcd for $C_{39}H_{27}Fe_2N_2O_7PS_2 \cdot {}^1/_3CH_2Cl_2$: C, 54.25; H, 3.20; N, 3.32. Found: C, 54.24; H, 3.38; N, 3.38. IR (KBr, ν cm^{-1}): ν(CO) 2045.4, 1985.9, 1931.0; ν(C≡C) 2210.2; ν(NO_2) 1514.7, 1339.9.

Synthesis of [$(CH_3)_2NC_6H_4C{\equiv}CC_6H_4NO_2$-4] (13). Complex **13** was synthesized under typical conditions for Sonogashira cross-coupling: to a well-degassed solution of 1-iodo-4-nitrobenzene (1.0 mmol) and 4-ethynyl-*N*,*N*-dimethylbenzenamine (1.0 mmol) in 25 mL of THF/NEt_3 (5:1) were added successively $Pd(PPh_3)_2Cl_2$ (15 mg) and then CuI (5 mg). After stirring under an argon atmosphere at 40−50 °C overnight, the mixture was concentrated in vacuo, and the black residue was subjected to column chromatography on silica gel (CH_2Cl_2/petroleum ether) to give complex **14** as an orange solid (yield 90%). MS (*m*/*z*): 266 [M^+]. ^{1}H NMR ($CDCl_3$, 400 MHz, δ ppm): 8.18 (d, J = 8.9 Hz, 2H), 7.59 (d, J = 8.9 Hz, 2H), 7.42 (d, J = 8.9 Hz, 2H), 6.67 (d, J = 8.9 Hz, 2H), 3.02 (s, 4H).

Synthesis of [$(CH_3)_2NC_6H_4C{\equiv}CC_6H_4CHO$-4] (14). Complex **14** was synthesized by a procedure similar to that for **13**, except that 4-bromobenzaldehyde (1.0 mmol) and 4-ethynyl-*N*,*N*-dimethylbenzenamine (1.0 mmol) were used. The mixture was concentrated in vacuo and subjected to column chromatography on silica gel (CH_2Cl_2/petroleum ether) to give complex **14** as a yellow solid (yield 65%). MS (*m*/*z*): 249 [M^+]. ^{1}H NMR ($CDCl_3$, 400 MHz, δ ppm): 9.93 (s), 7.83 (d, J = 8.2 Hz, 2H), 7.62 (d, J = 8.1 Hz, 2H), 7.43 (d, J = 8.7 Hz, 2H), 6.70 (d, J = 8.5 Hz, 2H), 3.02 (s, 4H).

X-ray Crystal Structural Determination. Diffraction measurements were made on a Bruker Smart 1000 X-ray diffractometer using graphite-monochromated Mo Kα radiation (λ = 0.71073 Å). Absorption correction was performed by the *SADABS* program.[22] The structure was solved by direct methods and refined by full-matrix least squares on F^2 using the *SHELXTL* crystallographic software package.[23,24] All hydrogen atoms were located by difference maps, and their positions were refined isotropically. All non-hydrogen atoms were refined anisotropically. Details of the crystal data and parameters for data collection and refinement are summarized in Table 1. Crystallographic data for **6**−**12**, **2**, and **3** have been deposited with the Cambridge Crystallographic Data Centre as supplementary publication CCDC nos. 643207−643213, 684670, and 684671, respectively.

Result and Discussion

Synthesis and Characterization. The syntheses of the designed complexes were carried out under typical Sonogashira coupling conditions (Scheme 1). The iodophenyl-substituted model complex of **1** was chosen to react with the 4-substituted phenylacetylene (HC≡CR) because of its higher reactivity over its bromophenyl-substituted counterpart. According to the procedure described by Rauchfuss,[10a,b] **1** was synthesized using lithium salt [(μ-LiS)$_2$Fe$_2$(CO)$_6$] (generated in situ from [(μ-S)$_2$Fe$_2$(CO)$_6$] and Et_3BHLi in THF at −78 °C) and *N*,*N*-bis(chloromethyl)-4-iodoaniline as the reagents. The reaction of **1** with HC≡CR in a mixed solvent of Et_3N and anhydrous THF, catalyzed by $Pd(PPh_3)_2Cl_2$ and CuI at 40−50 °C, afforded complexes **2**−**10** as red solids with good-to-excellent yields, respectively. The isolated yield of the complexes was found to rely on both the electronic effect of the R group and the temperature used. A stronger electron-accepting ability of the R group results in a higher yield of the phenylacetylene-functionalized Fe_2S_2 model complex. Increasing the reaction temperature also leads to a much higher obtained yield. When the reaction temperature was increased from room temperature to 40−50 °C, the isolated yield of **2** with an electron-poor nitro group was enhanced and ranged from 78% to 90%. Moreover, the facile cross-coupling reactions of phenylacetylene bearing an amino or carboxylic group with **1** suggest that the model complexes with different functional groups do not suffer from the competition for their potential ability to bind the metal in preference to the ligands. Compared with aniline- and benzaldehyde-functionalized complexes in the literature,[12c,d] the synthesis can be performed under mild conditions with a shorter reaction time but higher yield. These results indicate that the protocol can tolerate a range of electron-donating and electron-accepting groups, even coordinative functional groups like amino, aldehyde, or carboxylic acid, which are amenable to either a photochemical active species or to electrode surfaces.

The electron-donating phosphine ligands have been known[5] to render two iron active centers of Fe_2S_2 model complexes more nucleophilic, thereby leading to effective electrocatalysts for proton reduction in the presence of acid. To examine whether the introduction of the acetylene moiety could influence the coordinated phosphine ligand, complex **11** was used as an example to react with 4-nitrophenylacetylene. The reaction was

(22) Sheldrick, G. M. *SADABS, A Program for Empirical Absorption Correction of Area Detector Data*; University of Göttingen: Göttingen, Germany, 1996..

(23) Sheldrick, G. M. *SHELXS97, A Program for Crystal Structure Solution*; University of Göttingen: Göttingen, Germany, 1997.

(24) Sheldrick, G. M. *SHELXL97, A Program for Crystal Structure Refinement*; University of Göttingen: Göttingen, Germany, 1997.

Table 1. X-ray Crystallographic Data for Complexes **4**−**12**[a]

complex	**2**	**3**	**6**	**7**	**8**
formula	$C_{22}H_{12}Fe_2N_2O_8S_2$	$C_{23}H_{13}Fe_2NO_7S_2$	$C_{25}H_{17}Fe_2NO_8S_2$	$C_{22}H_{12}FFe_2NO_6S_2$	$C_{22}H_{13}Fe_2NO_6S_2$
fw [g mol^{-1}]	608.16	591.16	635.24	581.15	563.15
T [K]	294(2)	294(2)	293(2)	294(2)	294(2)
cryst syst	triclinic	triclinic	orthorhombic	monoclinic	monoclinic
space group	$P\bar{1}$	$P\bar{1}$	$P2_12_12_1$	$P2_1/n$	$P2_1/n$
a (Å)	7.6369(18)	7.7210(18)	9.1855(18)	7.8472(14)	7.9750(13)
b (Å)	9.177(2)	11.982(3)	10.272(2)	9.2944(17)	9.4039(15)
c (Å)	19.010(4)	13.369(3)	28.470(6)	32.124(6)	32.050(5)
α (deg)	84.110(4)	88.743(4)	90	90	90
β (deg)	87.509(4)	78.900(3)	90	91.196(3)	91.499(3)
γ (deg)	65.421(3)	78.787(4)	90	90	90
V [Å^3]	1205.2(5)	1190.4(5)	2686.2(9)	2342.5(7)	2402.8(7)
cryst size [mm]	0.22 × 0.20 × 0.12	0.24 × 0.20 × 0.14	0.22 × 0.20 × 0.16	0.32 × 0.20 × 0.16	0.20 × 0.18 × 0.18
reflns collected	6848	6083	16 758	12 805	13 144
indep reflns	4896	4162	4701	4777	4879
GOF (on F^2)	1.094	1.028	1.055	1.094	1.229
final R indices [$I > 2\sigma(I)$]	R1 = 0.0323, wR2 = 0.0840	R1 = 0.0356, wR2 = 0.0824	R1 = 0.0344, wR2 = 0.0813	R1 = 0.0426, wR2 = 0.0867	R1 = 0.0533, wR2 = 0.1272
R indices (all data)	R1 = 0.0417, wR2 = 0.0885	R1 = 0.0567, wR2 = 0.0934	R1 = 0.0383, wR2 = 0.0838	R1 = 0.0624, wR2 = 0.0935	R1 = 0.0636, wR2 = 0.1311
Z	2	2	4	4	4
ρ_{calcd} (g/m^3)	1.676	1.649	1.571	1.648	1.557
F(000)	612	596	1288	1168	1136
θ range (deg)	1.08−26.51	2.31−25.01	2.11−24.99	1.27−26.41	1.27−26.47
μ(Mo Kα) [mm^{-1}]	1.428	1.439	1.284	1.464	1.418
no. of param	325	316	345	307	298
largest diff peak and hole [e/Å^3]	0.320 and −0.360	0.287 and −0.430	0.324 and −0.343	0.247 and −0.406	0.398 and −0.522

complex	**9**	**10**	**11**	**12**
formula	$C_{23}H_{15}Fe_2NO_7S_2$	$C_{44}H_{39}ClFe_2N_4O_6S_2$	$C_{31}H_{23}Fe_2INO_5PS_2$	$C_{40}H_{29}Cl_2Fe_2N_2O_7PS_2$
fw [g mol^{-1}]	593.18	931.08	823.19	927.34
T [K]	143(2)	293(2)	294(2)	294(2)
cryst syst	monoclinic	triclinic	triclinic	monoclinic
space group	$P2_1/c$	$P\bar{1}$	$P2_1/c$	$P2_1/c$
a (Å)	10.467(2)	8.4258(17)	9.530(2)	10.550(9)
b (Å)	9.1330(18)	9.934(2)	10.208(2)	14.781(12)
c (Å)	26.078(5)	26.979(5)	17.497(4)	26.04(2)
α (deg)	90	91.19(3)	73.396(4)	90
β (deg)	98.06(3)	98.12(3)	79.637(4)	99.951(15)
γ (deg)	90	97.05(3)	87.400(4)	90
V [Å^3]	2468.3(9)	2216.9(8)	1604.6(6)	4000(6)
cryst size [mm]	0.45 × 0.28 × 0.20	0.14 × 0.12 × 0.10	0.26 × 0.24 × 0.20	0.26 × 0.22 × 0.16
reflns collected	13 878	13 649	8361	20 551
indep reflns	5172	7737	5622	7080
GOF (on F^2)	1.001	0.976	1.048	0.992
final R indices [$I > 2\sigma(I)$]	R1 = 0.0382, wR2 = 0.0937	R1 = 0.0424, wR2 = 0.0958	R1 = 0.0382, wR2 = 0.0932	R1 = 0.0497, wR2 = 0.1181
R indices (all data)	R1 = 0.0584, wR2 = 0.1042	R1 = 0.0649, wR2 = 0.1083	R1 = 0.0548, wR2 = 0.1036	R1 = 0.1124, wR2 = 0.1503
Z	4	2	2	4
ρ_{calcd}(g/m^3)	1.596	1.404	1.704	1.540
F(000)	1200	966	816	1888
θ range (deg)	1.18−26.40	1.53−25.02	2.08−25.02	1.59−25.02
μ(Mo Kα) [mm^{-1}]	1.388	0.860	1.439	1.056
no. of param	318	557	388	515
largest diff peak and hole [e/Å^3]	0.325 and −0.364	0.383 and −0.310	0.704 and −1.443	0.406 and −0.648

[a] $R1 = \sum||F_o| - |F_c||/\sum|F_o|$ and $wR2 = [\sum(|F_o^2 - F_c^2|)^2/\sum(wF_o^2)^2]^{1/2}$.

performed in a well-degassed THF/NEt_3 solution in the presence of $Pd(PPh_3)_2Cl_2$ and CuI. The resulting mixture was stirred for 3 h and concentrated in vacuo. The black residue was subjected to column chromatography on silica gel (CH_2Cl_2/petroleum ether) to give **12** as a red solid in 82% yield (Scheme 2). Obviously, the Sonogashira cross-coupling reaction is effective for modification of Fe_2S_2 model complexes.

IR and ^{1}H and ^{13}C NMR spectroscopies, MS spectrometry, and satisfactory elemental analyses confirmed the identities of the complexes studied in this work. Unlike the triple bond, which exhibits weak absorption at around 2210 cm^{-1}, several strong absorption bands ranging from 2085 to 1960 cm^{-1} dominate the IR spectra of the series **2**−**10**, which are the typical stretching of the coordinated CO around the Fe−Fe metal core. The similarity of **1** and the other all-carbonyl derivatives implies that the Sonogashira reaction would not interfere with the electron distribution of the coordination sphere. Consistent with the more nucleophilic metal core that the PPh_3 ligand made in **11** and **12**, the electron-donating phosphine ligands shift the strong absorption bands of the coordinated CO groups to low frequencies at about 30 cm^{-1}. In addition, the absorption associated with the aldehyde, amino, or carboxylic acid group in **3**−**5** appeared at 1660.5, 3411.6, and 3414.8 cm^{-1}, respectively.

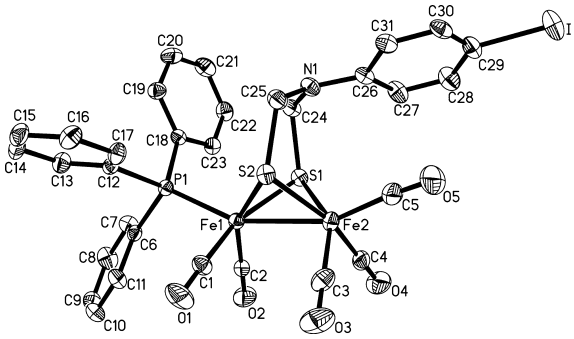

Figure 3. ORTEP view of **11** (ellipsoids at the 30% probability level).

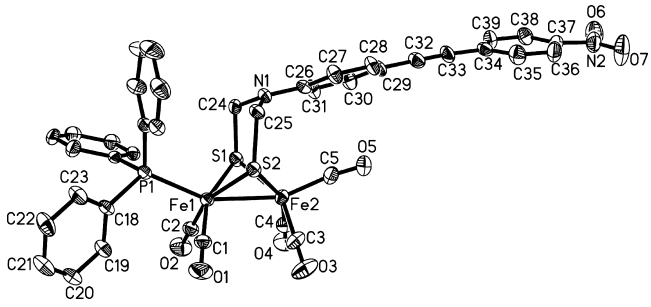

Figure 4. ORTEP view of **12** (ellipsoids at the 30% probability level).

Compared with that for **1** (4.28 ppm), the chemical shifts of **2**−**10** for their CH_2 groups on the adt bridge shift to a relatively lower field at 4.33−4.60 ppm. The downfield shifts suggest that the electronic communication between the N-bridged phenyl ring and phenylacetylene indeed takes place. Owing to delocalization, the electron density on the nitrogen heteroatom of **2**−**10** is much decreased. Complexes **11** and **12** with electron-donating PPh_3 ligands exhibit two respective doublets at 3.0 and 4.0 ppm for their CH_2 groups on the adt bridge, reflecting that the bulky PPh_3 and diphenylacetylene fix the conformation of Fe_2S_2 model complexes and make the CH_2 groups on the adt bridge chemically unequivalent.

Crystal Structural Analysis. The crystal structures of **2**, **3**, and **6**−**12** were further determined by X-ray diffraction. Single crystals of **2**, **3**, and **6**−**12** have been obtained by immersion of hexane into a CH_2Cl_2 solution. Dark-red single crystals as plates were used for data collection on a Bruker Smart 1000 X-ray diffractometer. The molecular structures of **3**, **6**, **11**, and **12** are shown in Figures 1−4, and the others are depicted in the Supporting Information (Figures S1−S5). Similar to the reported [(μ-adt)$Fe_2(CO)_6$] analogues,[12] the two iron atoms and the two sulfur atoms form a butterfly conformation, in which the metal atoms are connected to each other through a Fe−Fe single bond and the aryl group on the N1-bridged atom slants to one iron site as a result of the two fused six-membered rings: N1C7S1Fe2S2C8 and N1C7S1Fe1S2C8. The C≡C bond length of ca. 1.2 Å is within the expected range, and its angle is nearly 180°. As expected, the linear and rigid triple bonds offer excellent control over the distance between the functional group and the active site of Fe_2S_2 model complexes. No binding of the introduced functionality to the iron core takes place (Figures 1−4 and S1−S5 in the Supporting Information). The sum of the C−N−C angles around the N1-bridged atom equals about 355°, suggesting that the p−π electron communication between the substituted phenyl ring and the p orbital of the nitrogen atom is somewhat weakened (Tables S1−S9 in the Supporting Information). It is apparent that the bulky PPh_3 ligand fixes the chair conformation of Fe1S1C24N1C25S2 in **11** and **12** (Figures 3 and 4), giving rise to the CH_2 group on the adt bridge being chemically unequivalent in ^{1}H NMR spectroscopy. Moreover, the hindrance also makes the respective P1−Fe1−Fe2 angles of 156.43(4)° for **11** and 155.03(5)° for **12** 10° larger than those found in the all-carbonyl-substituted analogues of **2**, **3**, and **6**−**12** (Tables S1−S9 in the Supporting Information).

It is worth noting that the Fe−Fe distance of 2.5888(9) Å in **6** is comparable to that of the enzyme in nature, while the others are in the range 2.5025(7)−2.5313(10) Å, shorter than that in *C. pasteurianum*[2a] and *D. desulfuricans*[2b] (ca. 2.6 Å) (Tables S1−S9 in the Supporting Information). The three angles around the N1-bridged atom [C9−N1−C7, 114.3(3)°; C7−N1−C8, 108.8(3)°; C9−N1−C8, 133.5(3)°] and the torsion angle of 105.81(5)° (S2−Fe1−Fe2−S1) in **6** are distinctly different from those existing in **2**, **3**, and **7**−**10** (Figure 2 and Tables S1−S9 in the Supporting Information). Each molecule of **6**, serving as both a hydrogen-bond donor and acceptor in the strong intermolecular C−H···O and C−H···S hydrogen bonds, stacks with the other four adjacent molecules in the molecular packing (Figure 5). The H···O distance (2.532 Å) in the C−H···O hydrogen bonding observed is appreciably shorter than the sum of the van der Waals radii for H (1.20 Å) and O (1.52 Å) with a C−H···O angle of 146.2°, and the H···S distance (2.881 Å) in the C−H···S interaction is remarkably shorter than the sum of the van der Waals radii for H (1.20 Å) and S (1.80 Å) with a C−H···S angle of 100.3°, respectively. The intriguing intermolecular contacts lead to a highly distorted structure, giving rise to the unusual Fe−Fe distance and the angles found in the molecular packing of **6**. The C−H···S hydrogen-bonding interaction, to the best of our knowledge, has not been realized in the Fe_2S_2 model complexes, albeit Novoa et al.[25] discussed its significance in the self-organization of crystals in 1995. Such an interaction is reminiscent of the protonation of the sulfur atom in Fe_2S_2 model complexes for catalytic H_2 evolution.[26]

Electrochemistry. To evaluate the redox properties of the model complexes, a cyclic voltammetric study of **2**−**12** was performed in a CH_3CN or DMF solution with 0.1 M nBu$_4$NPF$_6$ as the supporting electrolyte and a 100 mV/s scan rate. The electrochemical data of the complexes are listed in Table 2. All of the cyclic voltammograms for **2**−**10** display irreversible oxidation and quasi-reversible and ir-

(25) For studies on the C−H···S hydrogen bond, see: (a) Novoa, J. J.; Carme Rovira, M.; Rovira, C.; Tarres, J. *Adv. Mater.* **1995**, *7*, 233–237. (b) Rovira, C.; Novoa, J. J. *Chem. Phys. Lett.* **1997**, *279*, 140–150.

(26) (a) Tard, C.; Liu, X.; Ibrahim, S. K.; Bruschi, M.; De Gioia, L.; Davies, S.; Yang, X.; Wang, L.-S.; Sawers, G.; Pickett, C. J. *Nature* **2005**, *443*, 610–613. (b) Cao, Z.; Hall, M. B. *J. Am. Chem. Soc.* **2001**, *123*, 3734–3742. (c) Greco, C.; Zampella, G.; Bertini, L.; Bruschi, M.; Fantucci, P.; De Gioia, L. *Inorg. Chem.* **2007**, *46*, 108–116. (d) Borg, S. J.; Tye, J. W.; Hall, M. B.; Best, S. P. *Inorg. Chem.* **2007**, *46*, 384–394.

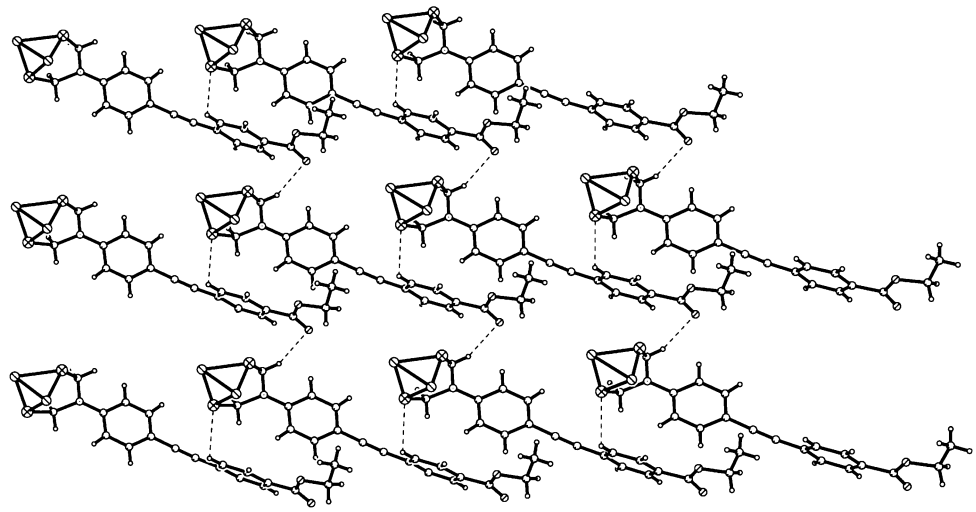

Figure 5. Molecular packing of **6**. The coordinated CO groups are omitted for clarity.

Table 2. Electrochemical Data of Complexes **2**−**12**[a]

complex	E_{pa}^1 [V]	E_{pa}^2 [V]	E_{pc}^1 [V]	E_{pc}^2 [V]
2[b]		+0.55	−1.56	
3[c]		+0.61	−1.56	−1.98
4[c]	+0.23	+0.46	−1.58	−2.06
5[d]		+0.64	−1.59	−2.49
6[c]		+0.60	−1.56	−2.08
7[c]		+0.57	−1.56	−2.08
8[c]		+0.55	−1.54	−1.99
9[c]		+0.55	−1.56	−2.03
10[c]	+0.20	+0.50	−1.55	−2.02
11[b]		+0.44	−1.67	
12[b]		+0.52	−1.67	

[a] All potentials are given versus Fc/Fc^+ (reference electrode: Ag/Ag^+ electrode, 10 mM of $AgNO_3$). Scan rate: 100 mV/s. Note: ferrocene exhibits its $E^{1/2}$ at ca. 0.09 V with reference to the Ag/Ag^+ reference electrode in the experiment. [b] 0.5 mM of model complex, 0.1 M nBu$_4$NPF$_6$ in CH_3CN. [c] 1.0 mM of model complex, 0.1 M of nBu$_4$NPF$_6$ in CH_3CN. [d] 1.0 mM of **5**, 0.1 M of nBu$_4$NPF$_6$ in DMF.

reversible reduction peaks. With reference to the previous works on all-carbonyl-substituted Fe_2S_2 model complexes,[10−12] the quasi-reversible and irreversible reduction peaks appearing in the ranges of −1.54 to −1.59 and −1.99 to −2.49 V vs Fc/Fc^+ are assigned to $[Fe^IFe^I] + e^- \rightarrow [Fe^IFe^0]$ and $[Fe^IFe^0] + e^- \rightarrow [Fe^0Fe^0]$ reduction processes, respectively, while the irreversible oxidative potential at +0.54 to +0.64 V vs Fc/Fc^+ is attributed to the $[Fe^IFe^I] \rightarrow [Fe^IFe^{II}] + e^-$ one-electron oxidative process. It is evident that the N-bridged adt model complexes are more easily oxidized or reduced as compared to C-bridged all-carbonyl pdt diiron complexes ($E_{ox} = 0.84$ V and $E_{red} = -1.57$ V vs Ag/Ag^+).[3b] Irreversible oxidation peaks at 0.23 and 0.20 V for **4** and **10**, respectively, were observed. The absence of this peak in the other studied **2**, **3**, and **5**−**9** complexes implies that oxidation of the amino group in **4** and **10** occurs. Upon incorporation of the electron-donating phosphine ligand into the Fe_2S_2 model complexes, the first reduction potential of **11** and **12** shifts to a more negative value around −1.67 V by 130 mV. In contrast, the first oxidative potential occurs at 0.44 and 0.52 V for **11** and **12**, respectively (Table 2). These results suggest that the electron-donating phosphine ligand makes reduction of Fe_2S_2 model complexes more difficult but oxidation easier.

The electrochemical behavior of catalytic proton reduction by **2**−**12** was investigated in the presence of weak acid of HOAc. For comparison, the electrolysis of HOAc was also measured. Controlled-potential electrolyses of all complexes were carried out to confirm H_2 evolution in the process of electrochemical reduction. Indeed, gas generation was clearly observed at around −2.10 V, while in the absence of the complexes, the reduction of HOAc is slow at this potential. Gas chromatography analyses of the reaction demonstrate that H_2 is produced during electrolysis. Consistent with bulk electrolysis, the addition of HOAc/CH_3CN to a solution of **2**−**12**, monitored by cyclic voltammetry, shows the characteristics of proton reduction.[27] As a representative, the electrochemical performance of **7** is given in Figure 6. Upon the addition of 2 mM HOAc to the CH_3CN solution of **7**, the current intensity of the first reduction peak of **7** at −1.56 V increases slightly and ceases to grow further with sequential increments of the acid concentration. However, the height of the second reduction peak at −2.03 V shows a linear dependence on the concentration of HOAc, indicating that the fully reduced $[Fe^0Fe^0]$ level is active for electrocatalytic H_2 evolution. Similar behaviors were also evidenced in the other complexes of **4**−**6** and **8**−**10**.

Notably, the proton reduction behavior of **2** and **12**, in which the R substituent carries a NO_2 group, is unique compared with the others studied in this work. The first irreversible peak for both **2** and **12** is gradually anodic shifted to −1.33 V vs Fc/Fc^+ upon the addition of HOAc, while the second quasi-reversible reduction peak appears with an increased current intensity (Figure 7). Consistent with the relative pK_a values of HOAc (pK_a = 22.3 in CH_3CN)[19] and of the protonated nitrogen bridgehead atom of closely related compounds,[10b] the N-bridged atom in the phenylacetylene-functionalized adt complexes cannot to be protonated by a weak acid of HOAc, even at high concentration. Therefore, the proton reduction of **2** and **12** under these conditions first requires an electron-transfer step!

(27) Bhugun, I.; Lexa, D.; Saveant, J.-M. *J. Am. Chem. Soc.* **1996**, *118*, 3982–3983.

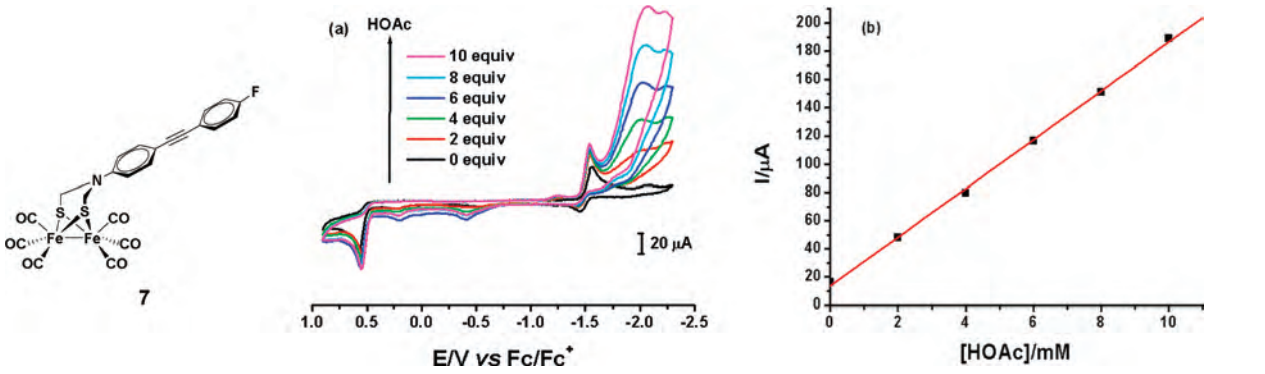

Figure 6. (a) Cyclic voltammograms of **7** (1.0 mM, 0.1 M of nBu$_4$NPF$_6$ in CH$_3$CN at a scan rate of 100 mV/s) in the presence of HOAc. (b) Dependence of the current height of the second reduction peak of **7** (1.0 mM) on the concentration of HOAc.

Considering that the electroreductively active nitro group is prone to being reduced, the enhanced current at a potential substantially less negative than that of [Fe^{I}Fe^{I}] + e$^-$ → [Fe^{I}Fe^{0}] for **2** and **12** is expected to be the result of a proton-dependent reduction of the nitro group in the adt-bridged complexes, as supposed by Talarmin and co-workers.[10i] Because the electrochemical reduction potential is significantly dependent on the functional-group-involved molecular structure, a rigid phenylacetylene-modified reference compound of **13** was prepared to shed light on the unique electrochemical behavior. Figure 8b shows the cyclic voltammetry of reference **13** in a CH$_3$CN solution. Obviously, the reduction potential of the nitro group appears at −1.47 V, which is overlapped with that of [Fe^{I}Fe^{I}] + e$^-$ → [Fe^{I}Fe^{0}] in the adt-bridged complexes. More importantly, with the addition of 6 equiv of HOAc to a solution of **13** in CH$_3$CN/nBu$_4$NPF$_6$, a reduction peak around −1.39 V arises. Clearly, the electrochemical behavior of **13** evidences the participation of the nitro group; namely, the reduction of the nitro group is followed by the protonation occurring at the reduced nitro species rather than at the Fe−Fe bond, thus shifting the reduction peak to a less negative potential in **2**. This observation is further strengthened by the fact that the peak around −1.33 V increases when HOAc is added to the solution of the PPh$_3$-substituted complex of **12** (Figure 7c), of which the two iron active centers are more nucleophilic with [Fe^{I}Fe^{I}] + e$^-$ → [Fe^{I}Fe^{0}] appearing at −1.67 V. With only the [Fe^{I}Fe^{I}] + e$^-$ → [Fe^{I}Fe^{0}] shifts to more negative potential, a similar electrocatalytic behavior of **2** and **12** was observed for proton reduction in the presence of HOAc. Therefore, reduction of the nitro group should be taken into consideration during a cyclic voltammetry scan for hydrogen production.

The occurrence of nitro group reduction in **2** and **12** prompts us to investigate the electrocatalyzed proton reduction of the other adt model complexes studied in this work. The process observed at around −1.3 V for **2** and **12** is not present for the others, while reduction at −1.54 V for [Fe^{I}Fe^{I}] + e$^-$ → [Fe^{I}Fe^{0}] is instead as the first reduced species. However, the current and potential of the second reduction peak are also dependent on the nature of the R substituent. When the aldehyde functionality is incorporated, the second reduction peak for **3** in the presence of HOAc has an anodic shift to −1.94 V with much higher current during a cyclic voltammetry scan (Figure 8). Such a phenomenon is well interpreted by the fact that the reduction potential of **14** (−2.07 V vs Fc/Fc$^+$) is overlapped with that of the [Fe^{I}Fe^{0}] + e$^-$ → [Fe^{0}Fe^{0}] process and gradually moves toward the less negative potential at −1.81 V upon the addition of HOAc in a CH$_3$CN solution.

On the basis of the above results, it could be speculated that the electrocatalyzed proton reduction observation involves a contribution from the electrochemically active group in the series of adt complexes. The reduction potential for the electron-transfer step can be altered by the functionality R. Complexes of **2** and **12**, with the electron-poor nitro group, display the enhanced current at a potential substantially less negative than the reduction of [Fe^{I}Fe^{I}] + e$^-$ → [Fe^{I}Fe^{0}]; that is to say, the reduction of the nitro group is most accessible and becomes the initial reduction step. For complex **3**, the second reduction peak for the electron-transfer step involves a contribution from the aldehyde functionality. As the electroreductively inactive groups are incorporated, the reduction process of [Fe^{I}Fe^{I}] + e$^-$ → [Fe^{I}Fe^{0}] appears first and the second reduction peak for the electron-transfer step from the [Fe^{I}Fe^{0}] + e$^-$ → [Fe^{0}Fe^{0}] process for **4**−**10** is clearly observed. Therefore, the order of electron and proton uptake is closely related to the functionality R. Notwithstanding, HOAc is too weak to protonate the series of adt-bridged Fe$_2$S$_2$ complexes **2**−**12** and different reduction pathways can be followed, thus leading to electrocatalysis occurring at different reduction levels. The participation of an electrochemically active group in the electrocatalyzed proton reduction renders the mimic of Fe$_2$S$_2$ model complexes uneven. The reductive event observed in **2**, **3**, and **12** implicates that more side reactions must be seriously considered for designing the biomimetic catalysts of hydrogenases.

Conclusion

The Sonogashira reaction was employed to synthesize a series of adt-bridged Fe$_2$S$_2$ model complexes of hydrogenases. The synthesis can be performed under mild conditions with a relatively short reaction time, but the yields are higher than those reported in the literature. The linear geometry and rigidity of a triple bond act as an effective bridge to anchor a functionality ranging from electron-donating to electron-accepting, even coordination groups in the adt model complexes. X-ray crystal analysis of **2**, **3**, and **6**−**12** reveals

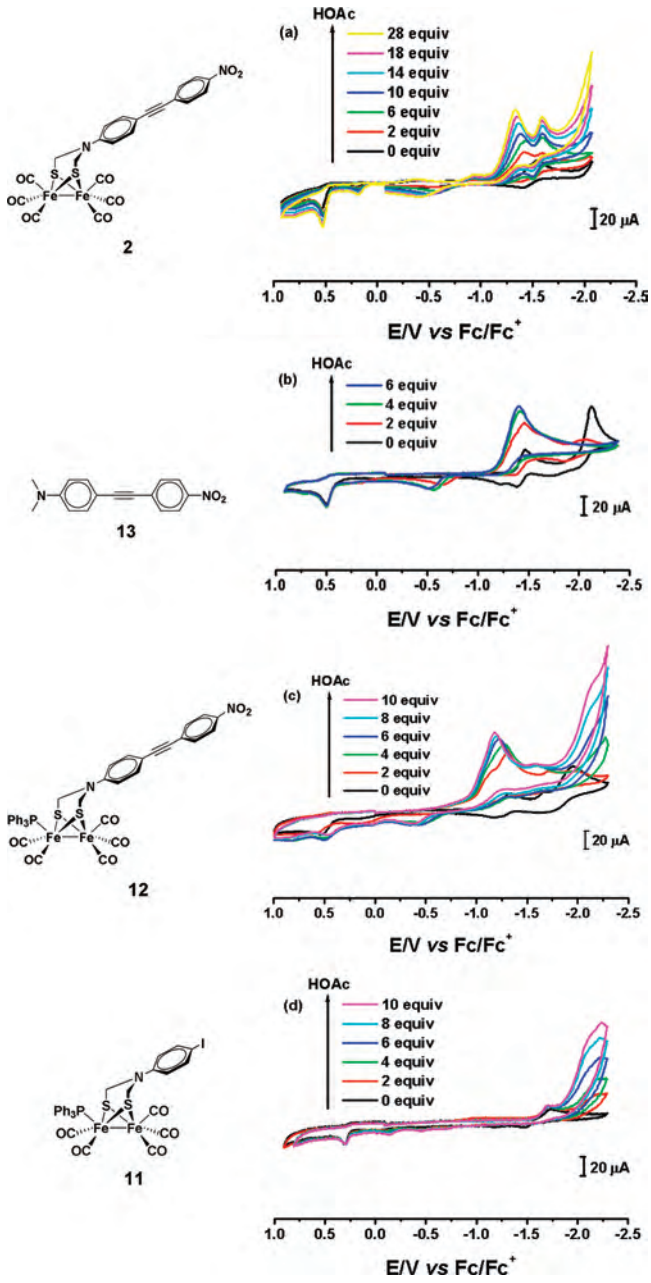

Figure 7. Cyclic voltammograms of **2** and **11**−**13** (0.5 mM, 0.1 M of nBu$_4$NPF$_6$ in CH$_3$CN at a scan rate of 100 mV/s).

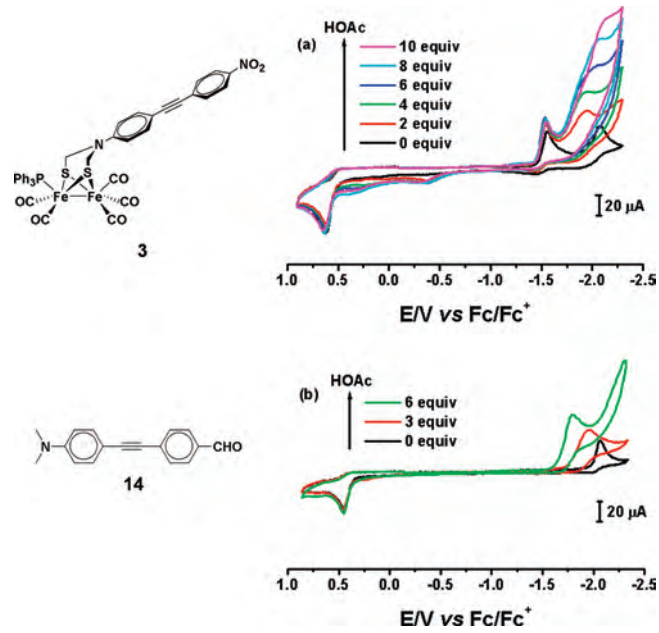

Figure 8. Cyclic voltammogram of **3** and **14** (1.0 mM, 0.1 M of nBu$_4$NPF$_6$ in CH$_3$CN at a scan rate of 100 mV/s).

that the model complexes retain the butterfly structure of Fe_2S_2 model analogues. A rigid phenylacetylene offers excellent control over the distance between the functional group and the active site of Fe_2S_2 model complexes. The unusual Fe−Fe distance and the angles were found to originate from the intriguing intermolecular C−H···O and C−H···S interactions in the molecular packing of **6**. Such an interaction is reminiscent of the protonation of the sulfur atom in Fe_2S_2 model complexes for catalytic H_2 evolution. More interestingly, electrochemical investigations reveal that the reduction potential for the electron-transfer step can be remarkably altered by the functionality R. The electron-poor nitro group in **2** and **12** displays the enhanced current at a potential substantially less negative than the reduction of $[Fe^IFe^I] + e^- \rightarrow [Fe^IFe^0]$, which is most accessible and becomes the initial step. For complex **3**, the second reduction peak for the electron-transfer step involves a contribution from the aldehyde functionality. As the electroreductively inactive groups are incorporated, the reduction process of $[Fe^IFe^I] + e^- \rightarrow [Fe^IFe^0]$ appears first and the second reduction peak for the electron-transfer step from the $[Fe^IFe^0] + e^- \rightarrow [Fe^0Fe^0]$ process for **4**−**10** is clearly observed. Therefore, the order of electron and proton uptake is closely related to the electroreductively active functionality R. Varying the nature of the functionality R leads to the electron-transfer step from the reduction of the electrochemically active R group to the active site of Fe_2S_2 model complexes. Notwithstanding, HOAc is too weak to protonate the series of **2**−**12**, different reduction pathways can be followed, and thus the electrocatalytic H_2 evolution occurs at different reduction levels. These results have illustrated that reduction of the electrochemically active group must be seriously considered for the mechanistic investigation during a cyclic voltammetry scan for hydrogen production. The easy modification of R and diverse electrocatalytic mechanisms open up interest in the adt-bridged Fe_2S_2 complexes for the construction of biomimetic catalyst systems.

Acknowledgment. We are grateful for financial support from the National Science Foundation of China (Grants 20333080, 20732007, 20728506, and 20672122), the Ministry of Science and Technology of China (Grants 2004CB719903, 2006CB806105, 2007CB808004, and 2007CB936001), and the Bureau for Basic Research of The Chinese Academy of Sciences.

Supporting Information Available: Crystallographic files of **2**, **3**, and **6**−**12** in CIF format, ORTEP views of **2** and **7**−**10**, and selected bond lengths and angles for complexes **2**, **3**, and **6**−**12**. This material is available free of charge via the Internet at http://pubs.acs.org.

IC800676Y